Enabling shear textures and fine-grained structures in Magnesium sheet by machining-based deformation processing

IOP Conf. Series: Materials Science and Engineering **63** (2014) 012155 doi:10.1088/1757-899X/63/1/012155

Enabling shear textures and fine-grained structures in Magnesium sheet by machining-based deformation processing

D Sagapuram[1,4], M Efe[2], KP Trumble[3,4] and S Chandrasekar[1,4]
[1]School of Industrial Engineering, Purdue University, West Lafayette, IN, USA
[2]Department of Metallurgical and Materials Engineering, Middle East Technical University, Ankara, Turkey
[3]School of Materials Engineering, Purdue University, West Lafayette, IN, USA
[4]Center for Materials Processing and Tribology, Purdue University, West Lafayette, IN, USA
E-mail: chandy@purdue.edu

Abstract. The production of Mg alloy AZ31B sheet in a single deformation step by large-strain extrusion machining (LSEM) is detailed. LSEM imposes intense simple shear in a narrow zone by constrained chip formation. The confined deformation and the associated *in situ* adiabatic heating are found to be the key factors in production of the Mg sheet without need for external (pre-) heating. A range of shear textures with basal planes inclined to the sheet surface are achieved by this processing. The basal plane inclination could be varied by controlling the strain path. Microstructures, both ultrafine-grained (100-500 nm) and conventional fine-grained (2-5 μm), have been obtained by controlling the adiabatic heating and the extent of dynamic recrystallization. The LSEM sheet with shear texture and fine grain size shows superior combinations of formability and strength compared to rolled sheet.

1. Introduction

Magnesium is an attractive material choice for structural applications because of its low density and reasonable strength. Wrought sheet form is of particular interest to the automotive and aerospace sectors, where weight reduction is critical. However, widespread usage of Mg is limited due to its poor ambient temperature formability – a result of limited slip systems, inherent to the hexagonal close-packed (h.c.p.) crystal structure. Strong crystallographic texture that develops during rolling further adversely affects the sheet formability. This texture, referred to as the basal texture, is characterized by the basal planes aligned parallel to the sheet surface. As a result, basal slip is restricted during sheet forming (zero resolved shear stress for slip) leading to premature fracture. Therefore, textures that are oriented favorably for basal slip are essential in order to improve the formability. It has been shown that textures in Mg can be modified by alloy/processing design [1]. For example, alloying Mg with rare earth elements was found to result in significantly altered textures with basal planes inclined to the sheet surface [1, 2]. Unfortunately, rare earth elements are expensive. The other approach is by shear-based thermo-mechanical processing using techniques such as equal channel angular pressing (ECAP) [3, 4], differential speed rolling (DSR) [5] and friction stir processing (FSP) [6]. The so-called tilted-basal textures achieved by these processes have been shown to significantly improve ductility, but usually at the cost of strength. Of these processes, only DSR is suitable for direct sheet production, albeit with a limited texture control.

In this study, the application of large-strain extrusion machining (LSEM) [7, 8], a shear-based deformation process, for the production of Mg sheet with controlled texture and microstructure is discussed. The deformation in LSEM is highly confined, which results in localized heating in the deformation zone and reduces the need for external heating in processing metals with poor workability (such as Mg). Concurrently, the severe plastic deformation (SPD) inherent to the process enables large grain refinement. Additionally, the strain path in LSEM can be conveniently varied, which offers opportunities for varying the sheet texture. These aspects of LSEM have been utilized to achieve novel combination of shear textures and fine-grained microstructures in Mg-3Al-1Zn (AZ31B) alloy sheet.

2. Large-Strain Extrusion Machining (LSEM)

2.1. Deformation Field and Strain Path

LSEM is a constrained chip formation process, wherein the sheet is formed under plane-strain deformation by simultaneous machining and extrusion. Figure 1a shows the (effective) strain-rate ($d\varepsilon/dt$) field in LSEM at a chip thickness ratio ($\lambda = t_c/t$) of 1; t_c is the final sheet thickness and t the undeformed chip thickness or feed. This strain-rate field was obtained using a high-speed image analysis technique, particle image velocimetry (PIV) [9, 10]. The region of high strain rate is the primary deformation zone, which is seen to be reasonably uniform and highly confined (50-100 μm thick). Velocity gradient measurements of this zone showed the deformation to be simple shear in nature. Figs. 1b and c show the strain rate and accumulated strain profiles along a pathline crossing the deformation zone. The deformation of an initial square element as it traverses the deformation zone is also shown in Fig. 1c. The associated strain, ε, rises steeply across the deformation zone before becoming constant. This constant value is the final strain imposed in the sheet. The strain of 1.2 measured from PIV is close to the estimated strain of 0.97 using ideal simple shear along plane OA:

$$\varepsilon = \frac{1}{\sqrt{3}}\left(\frac{\lambda}{\cos\alpha} + \frac{1}{\lambda\cos\alpha} - 2\tan\alpha\right) \tag{1}$$

where α is the tool rake angle (Fig. 1a). Strains in the present study are estimated to first order using Eq. 1.

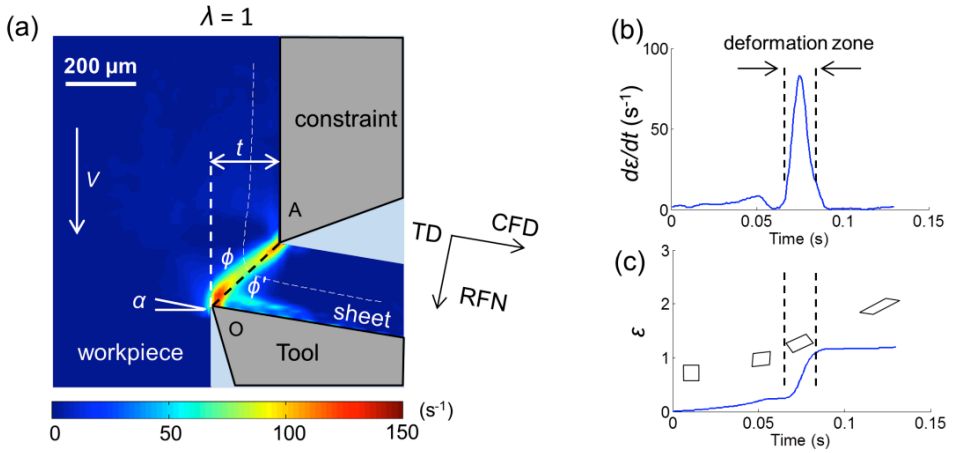

Figure 1. Deformation in LSEM: (a) strain-rate field showing the confined deformation zone; strain-rate (b) and accumulated strain (c) profiles along a pathline across the deformation zone. CFD is the chip flow direction, RFN the rake face normal and TD the transverse direction. Workpiece is commercially pure lead, $\lambda = 1$, $t = 200$ μm, $\alpha = 10^o$ and $V = 10$ mm/s.

Additional high-speed image analysis of LSEM at other constraint (λ) levels showed that the single shear plane model is a good approximation of the deformation [8]. The strain path for any deformation process, in theory, is defined by the velocity gradient field. Since the deformation in LSEM can be approximated as simple shear along a plane, strain path in the present case can be simply described by the velocity gradient or, equivalently, shear orientation in the middle of the primary deformation zone. For $\lambda = 1$, the (maximum) shear direction of 47^o (counter clockwise from the tool rake face) in the middle of the zone, measured using PIV, is in good agreement with the macroscopic shear plane angle, φ' (Fig. 1a), of 50^o given by:

$$\varphi' = \frac{\pi}{2} + \alpha - \varphi \quad (2)$$

where $\varphi = \tan^{-1}(\cos\alpha/(\lambda - \sin\alpha))$. This agreement was found to be valid also at other constraint levels, except at severe constraint levels ($\lambda \leq 0.5$) [8, 9]. Therefore φ' is used in this study for specifying the strain path. Since strain path is one of the key factors determining texture, the final sheet texture can be varied by controlling φ' (using either λ or α, Eq. 2).

2.2. Deformation Temperature

In LSEM, large adiabatic heating occurs in the deformation zone because of the highly localized plastic dissipation and high deformation rates (V ~ 0.25 to 4 m/s). The deformation (zone) temperature, T, is given by $T = T_o + \Delta T$, where T_o is the workpiece initial temperature and ΔT is the adiabatic temperature rise. ΔT can be estimated by measuring the specific shear energy of chip formation, u_s, and partitioning the heat between the chip (sheet) and workpiece. A detailed analysis of estimating the temperature rise, and its dependence on LSEM parameters, is presented elsewhere [7]. Prior work [7, 8] has shown that the temperature rise in LSEM can be substantial, for example, reaching up to 240°C in Mg under high deformation rates ($V >$ 1 m/s). These high levels of adiabatic heating are in fact found to be the key in the production of continuous Mg sheet forms with minimal external heating. Further control over the adiabatic heating by adjusting V is also quite useful for controlling the extent of dynamic recovery/recrystallization, and thereby the microstructure of the sheet.

3. Experimental

Mg AZ31B in the form of a rolled plate (6 mm thick) was obtained from ThyssenKrupp Materials NA, Inc. The starting material was characterized by a grain size of 15 μm and strong (10 mrd) basal texture. A disk workpiece of ~ 100 mm diameter was cut from the rolled plate for LSEM in a rotary configuration on a lathe [7, 8]. In this configuration, sheet is continuously "peeled" from the surface of a cylindrical shaped workpiece rotating at a constant surface velocity, V.

The deformation parameters varied in this study were the strain path and T. By keeping α fixed at 5° and varying λ between 0.5 and 1.4, a range of strain paths (φ' of 27-58°) was achieved. The variation of strain, ε, over the λ range of 0.5-1.4 is minimal ($<$ 25%, refer Eq. 1), and thus ε may be considered constant (~ 1) in this study. T was set in the range of 165-500°C by adjusting V and/or T_o. For setting T, u_s was measured for various deformation conditions by measuring the cutting force, F_c (parallel to the velocity direction), using a piezoelectric dynamometer.

Microhardness of the sheet specimens was measured by Vickers indentation at a load of 50 g. Transmission electron microscopy (TEM) samples were prepared by twin-jet electropolishing at 50 V using a solution of 1% percholric acid in ethanol at -20°C. Bright-field TEM images were obtained using an FEI Tecnai microscope at accelerating voltage of 200 kV. In each specimen, the average grain size was measured using the linear intercept method covering at least 500 grains from the optical microscopic images. In ultrafine-grained (UFG) specimens, grain size was measured by identifying at least 50 well-defined grains from the TEM images. Texture in the sheet was measured using an X-ray diffraction system equipped with an area detector (GADDS, Bruker AXS) and a Cu source [8]. The diffraction data was processed using a Rietveld refinement based software program, MAUD [11].

4. Results and Discussion

Since LSEM is a continuous process, it is critical to establish the microstructure of the material that enters the primary deformation zone, which may be different from the as-received material due to the deformation field of the advancing tool. An early set of experiments focused on characterizing the subsurface deformation in the workpiece revealed interesting results. For example, at λ = 1, an

unusually thick deformed layer (~ 2 mm) with a high density (~ 50%) of twins, underlying the machined surface was observed. Figure 2 shows the microstructure of this deep twinned layer. Electron backscattered diffraction analysis revealed the twins to be of the (10-12) type (Ref. [8]). The (10-12) twinning is consistent with the compressive stress field existing ahead of the deformation zone, and with the low strain (0.1-0.2) and high strain rate (~ 10^3 s^{-1}) conditions therein [12], known to be conducive for deformation twinning. It should be noted that (10-12) twinning results in reorientation of basal planes by ~ 86°. As a result, basal planes that are initially oriented parallel to the workpiece side surface in the as-received condition reorient to align nearly parallel to the machined surface after LSEM deformation.

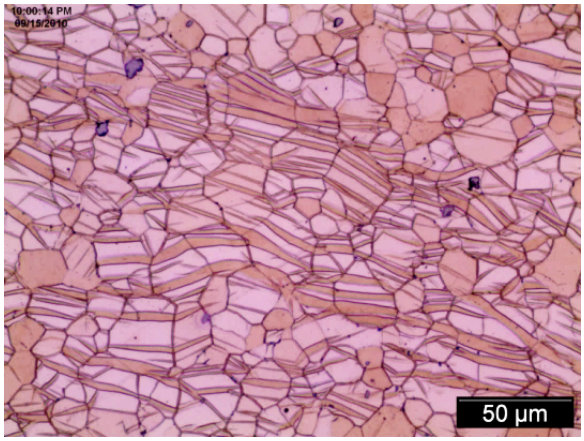

Figure 2. Subsurface twinned layer in the workpiece; $\lambda = 1$, $t = 250$ µm, $V = 1$ m/s and $T_o = 25^oC$.

While the surface deformation is intrinsic to machining, the observed subsurface structure modification over a layer of thickness ~ 10 times that of t in AZ31B is peculiar and unusually large compared to other metals [12]. This means that the texture of the material entering the deformation zone is different from the original texture in the starting workpiece material. As will be shown, this texture modification in the subsurface has a significant effect on the final sheet texture. The subsurface twinned layer was found to remain unchanged after two full workpiece revolutions. Hence, the sheet specimens selected for the characterization were taken after at least two revolutions.

4.1. Texture

Characteristic shear textures of LSEM sheet specimens are shown in Fig. 3. Figures 3a-c correspond to specimens processed at different constraint levels (λ = 0.6, 0.7 and 1.0, respectively), without pre-heating of the workpiece (i.e., $T_o = 25^oC$). The deformation (zone) temperature, T, for these conditions was estimated to be in the range of 175-240°C, with T increasing with the severity of the constraint level (decreasing λ) [8]. The textures are readily seen to be significantly different from the conventional rolling (basal) texture. Here, the major texture component has the basal poles inclined away from the sheet surface normal direction towards chip flow direction (CFD). The basal pole inclination in Figs. 3a-c is ~ 34-45°, depending on λ. According to the h.c.p. texture nomenclature [13], this component is referred to as the B-fiber. B-fiber occurs under simple shear deformation due to

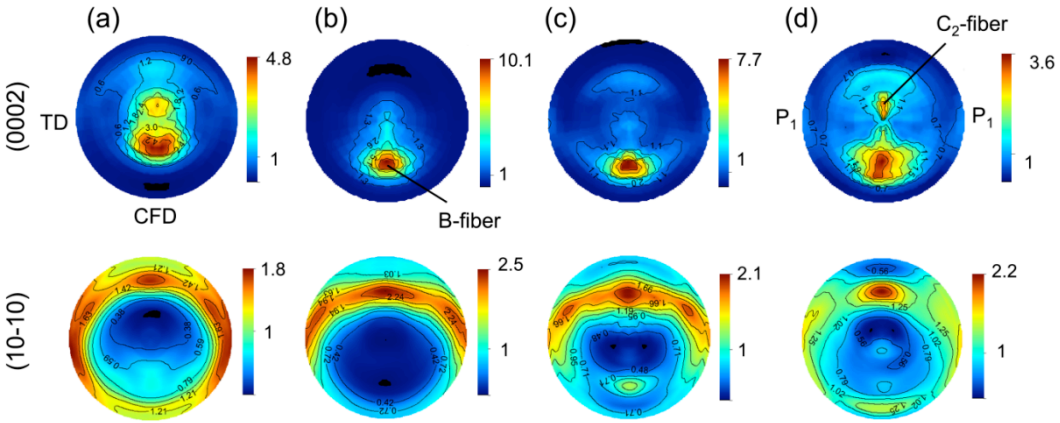

Figure 3. Pole figures obtained from the sheet surface showing texture dependence on λ and temperature: (a) $\lambda = 0.6$, $T_o = 25^oC$, (b) $\lambda = 0.7$, $T_o = 25^oC$, (c) $\lambda = 1.0$, $T_o = 25^oC$ and (d) $\lambda = 0.7$, $T_o = 200^oC$. Deformation rate, $V = 1$ m/s. B- and C_2-fibers, and P_1 component are highlighted for reference. The texture intensity is given in mrd (multiples of random distribution).

basal slip resulting in the basal plane alignment parallel to the shear plane. As will be detailed, deformation by basal slip in the primary shear zone in LSEM results in the alignment of basal planes with the macroscopic shear plane OA (Fig. 4b). The minor texture component with basal poles nearly parallel to the surface normal at $\lambda = 0.6$ (Fig. 3a) is due to the secondary shear, arising from frictional deformation between the outcoming sheet and tool rake face that occurs at low λ values [8]. Figure 3d shows the texture of sheet specimen processed at $\lambda = 0.7$ from a workpiece pre-heated to 200°C; corresponding T was estimated to be much higher, ~ 400°C. As evident from the figure, in addition to the B-fiber, an additional weak component with the basal poles inclined from the surface normal towards the negative CFD, is observed. This component resembles the C_2-fiber [13] associated with the pyramidal $<c+a>$ slip. Similar high temperature experiments at other constraint (λ) levels also yielded similar textures – primary B-fiber and a secondary C_2-fiber [8].

In the following, the observed texture components are interpreted in terms of slip mode activity dependence on initial texture and temperature, and the strain path.

4.1.1. Slip Activity

As shown in Fig. 3, warm T ($< 250^oC$) textures are characterized by a strong B-fiber, whereas at high T ($> 250^oC$), an additional minor C_2-fiber is observed. This indicates the basal slip to be the most active mode, whereas pyramidal $<c+a>$ slip is activated only at high T. Note that due to the subsurface twinning, as shown in Fig. 2, the material entering the shear zone has two texture components, corresponding to the parent and twinned volumes. Schmid factor calculations [8] for various slip modes under simple shear in LSEM showed that the parent volume is oriented primarily for prismatic and pyramidal $<a>$ slip. On the other hand, the twinning reorients the structure for basal and pyramidal $<c+a>$ slip. The appearance of only the B-fiber in the warm T shows the dominance of basal slip at these temperatures over other modes that are equally (geometrically) favorable, and is undoubtedly due to the low critical resolved shear stress (crss) for basal slip [14].

At elevated temperatures, the crss of secondary slip modes decreases and becomes nearly equal to that of basal slip. Hence, the appearance of C_2-fiber associated with the pyramidal $<c+a>$ slip, in the high T regime, is not surprising. The absence of texture fibers (P- and Y-) associated with prismatic and pyramidal $<a>$ slip is likely due to the low intensity of orientation stability parameter along these fibers [13]. The stable orientation along the P-fiber is its end orientation P_1 (see Fig. 3d). In fact, a faint intensity at P_1 can be seen, suggesting some activity of these modes as well. However, the reason for its low intensity compared to B- and C_2-fibers is not clear.

4.1.2. Strain Path

A key parameter that affects texture, besides slip activity, is the strain path. The effect of strain path on the sheet texture in LSEM can be described, for example, by examining the dependence of B-fiber orientation on λ. B-fiber orientation, θ_b, is defined as the basal pole inclination from the sheet surface normal, see Fig. 4b. The variation of θ_b (obtained from texture measurements) with λ is shown in Fig. 4a, where with increase in λ from 0.5 to 1.4, θ_b increases from 32 to 53°. As a reference, the variation of φ' with λ (Eq. 2) is also plotted in the figure. Note that θ_b and φ' are equivalent for the ideal B-fiber. The measured θ_b values are seen to fall closely along the φ' curve, confirming the alignment of basal planes with the LSEM shear plane. Indeed, this is to be expected since the LSEM strains (~ 1) are nearly sufficient to rotate the fibers to their ideal (end) positions.

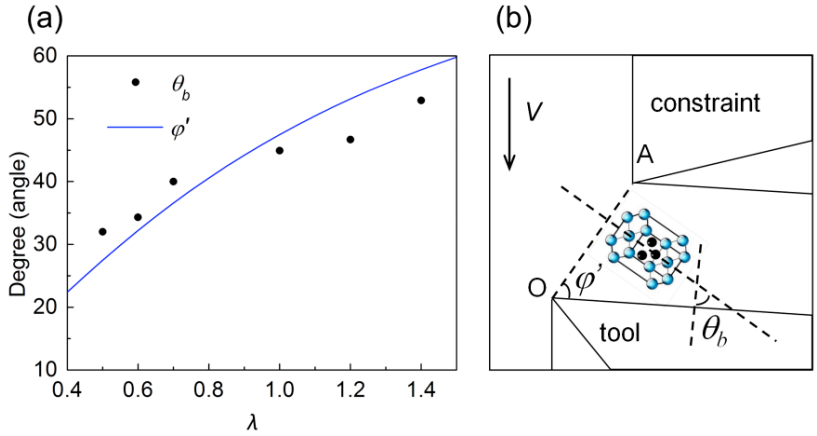

Figure 4. Strain path effect on texture in LSEM: (a) dependence of B-fiber orientation on λ; solid curve shows the φ' variation with λ; (b) schematic showing the alignment of basal plane parallel to the shear plane.

In summary, LSEM sheet is characterized by novel shear (tilted-basal) textures very different from that of rolled sheet; by varying the strain path (λ) and slip activity (dependent on initial texture and T), a range of textures can be achieved.

4.2. Microstructure, Grain Size and Hardness

Microstructural measurements were carried out on sheet specimens processed at a fixed $\lambda = 0.7$, corresponding to ε of 1.1 (Eq. 1). T was varied by adjusting V and T_o. Sheet was found to be segmented (discontinuous) below 140°C, which is believed to be due to limited slip activity at low T. The dependence of grain size (d) and hardness on T in the range 165-500°C is shown in Fig. 5 (the error bars denote the standard deviation). It is clear that a range of grain sizes (100 nm to 5 μm) can be achieved by controlling T. At T between 165 and 190°C, the microstructure was of cold-worked type typical of UFG samples, and often heterogeneous, consisting of sub-micron sized grains and dislocation substructures (for example, see Fig. 6a). Since only well-defined grains are considered in the grain size measurements, the sizes reported herein for the UFG samples should be treated as a lower bound. The UFG samples are characterized by a high hardness of 100-110 HV, nearly twice that of the starting material (58 HV). These hardness values are consistent with those previously reported for UFG Mg processed by other SPD processes [15, 16].

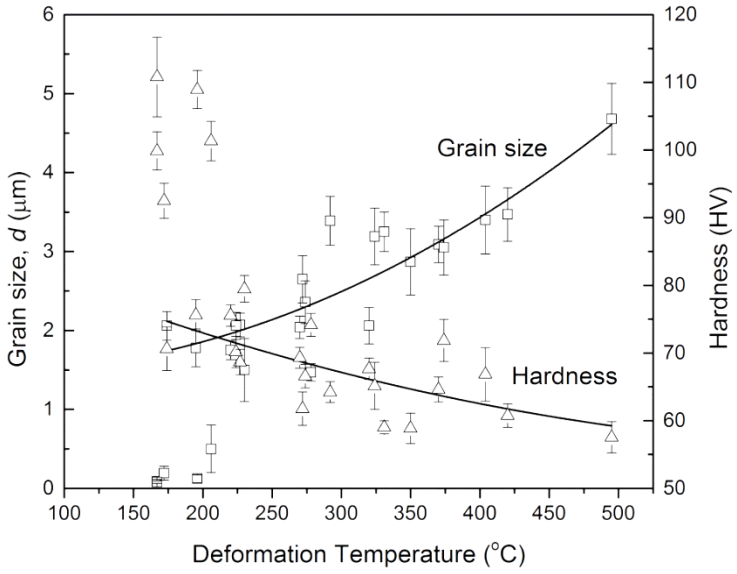

Figure 5. Variation of grain size (*d*) and hardness with deformation temperature, *T*. Lines (polynomial fit) drawn to guide the eye.

In a narrow *T* range of 200-225°C, a microstructural transition from cold-worked to fully recrystallized type takes place. From Fig. 5, it is evident that during this transition, the grain size increases sharply to ~ 1.5 μm, accompanied by a hardness decrease to ~ 80 HV. It is tempting to attribute this sharp transition in microstructure, grain size and hardness to the activation of discontinuous (dynamic) recrystallization, since it is well known that the classical recrystallization involving grain boundary bulging (nucleation) and migration (growth) leads to sharp changes in microstructure and strength. However, as will be shown, detailed TEM characterization of deformed structures revealed the recrystallization mechanism to be in fact of continuous type, involving recovery-based dislocation rearrangement and grain boundary formation. Above 225°C, the recrystallized grain size continuously increased with *T* (Fig. 5), this to be expected because of reduced defect densities at high temperatures in conjunction with a possible dynamic grain growth.

4.2.1. UFG Structure Formation and Dynamic Recrystallization

The UFG structure formation and the microstructural transitions from cold-worked to recrystallized type were investigated by varying *T* in the range 170-240°C and tracking the deformed microstructure and texture. The microstructural changes observed with increasing *T* are summarized in Fig. 6. At 170°C, cells ~ 100 nm in size with "fuzzy" boundaries are observed (Fig. 6a). The misorientation angle across these cell domains is expected to be quite low. The fine lamellae structures in Fig. 6a should not be confused with the deformation twins. High-resolution TEM studies have in fact showed these structures to be well-known Moiré fringes. Interestingly, samples processed in the temperature range of 160-180°C often also showed very fine (1-2 nm wide) stacking faults (not shown here), which also perhaps contribute to their high strength. With increase in *T* to 192°C, the boundaries become sharper (see contrast change at the arrows, Fig. 6b), likely due to the increased driving force for the dislocations to rearrange and form a boundary. Note that the grain size concurrently increased to ~ 200 nm and also the dislocation density inside the grains seems to have reduced. At 230°C, grains are seen to be depleted of dislocations (arrows, Fig. 6c), even though some random dislocation substructures still exist around these grains. Most grains have also coarsened to ~ 1 μm. At *T* of ~ 240°C, the microstructure transforms to fully recrystallized type (Fig. 6d) without apparent dislocation

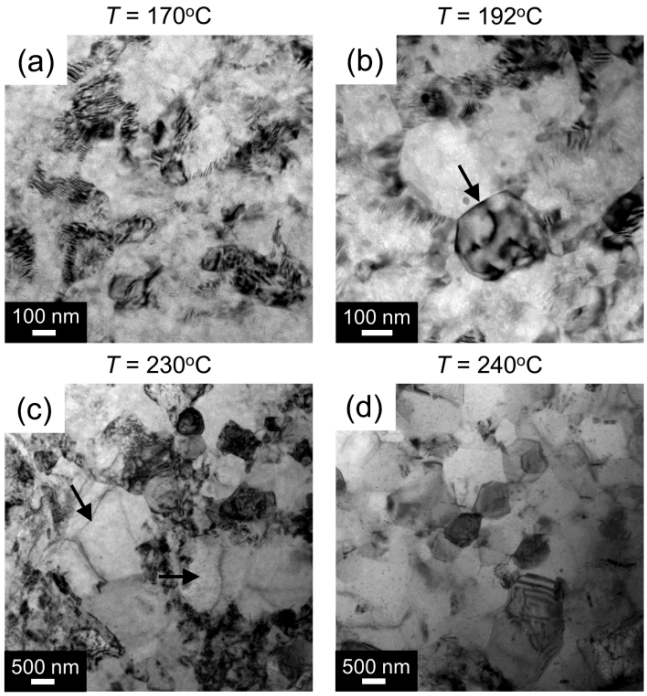

Figure 6. Bright-field TEM images showing the microstructural transitions with *T*. Note the different magnifications of the images.

substructures. Note also the close resemblance of grain boundaries with those seen in statically recrystallized (annealed) polycrystalline metals. This type of recovery-based grain refinement is known as the continuous (or "*in situ*") dynamic recrystallization, and is common in Mg [17].

Texture measurements of the specimens in Fig. 6 showed B-fiber to be the major texture component. As noted earlier, this is because of extensive basal slip at warm *T* ($< 250^{o}$C). However, a ~ 30^{o} rotation of the basal planes (about the *c*-axis) was observed between the cold-worked (Fig. 6a) and fully recrystallized (Fig. 6d) specimens. This type of 30^{o} rotation of basal planes upon recrystallization (both static and dynamic) is a characteristic feature of h.c.p. metals [18, 19].

As a note, the grain refinement seen here is greater than that observed in other SPD processes (e.g., ECAP) that impose similar strains in a single pass [4]. It is likely that prior subsurface deformation and twin formation in the LSEM play a role in enhancing the grain refinement.

4.2.2. Hall-Petch Strengthening

To illustrate the grain size effects on strength (hardness), the grain size-hardness data from Fig. 5 are plotted as a Hall-Petch (H vs. $1/d^{1/2}$) plot, as shown in Fig. 7. Such a plot yielded a straight line, confirming the widely known Hall-Petch relationship in metals. For grain sizes in the range 1.5-5 μm, the slope is ~ 69 kg/mm^2 μm$^{1/2}$, slightly higher than previously reported values of 40-50 kg/mm^2 μm$^{1/2}$ for AZ31B [20]. For sub-micron grain sizes, the slope is much lower (~ 24 kg/mm^2 μm$^{1/2}$). Such a decrease in the Hall-Petch slope with decreasing grain size, especially below 1 μm, is not uncommon. Indeed, at sub-micron grain sizes, deformation modes associated with grain boundaries and triple junctions such as grain boundary sliding and diffusion processes may compete with the dislocation slip in accommodating the imposed deformation, reducing the Hall-Petch slope.

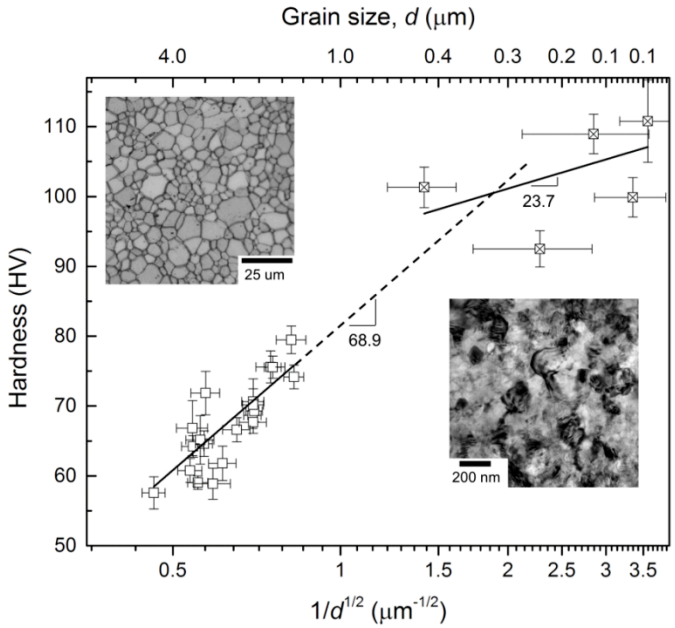

Figure 7. Hall-Petch plot showing the slope change in the sub-micron grain size regime. Characteristic microstructures corresponding to fine-grained and UFG regimes are shown.

5. Implications for Mechanical Properties

It has been shown that sheet produced by LSEM is primarily characterized by B-fiber texture (Fig. 3) with controllable basal plane inclination. This is a consequence of the simple shear deformation in LSEM wherein the orientation of the shear can be varied by adjusting λ. Since basal slip is the main deformation mode in Mg at ambient temperatures, a higher level of sheet ductility/formability should be realized when basal planes are inclined from the sheet surface with a high Schmid factor for basal slip. In fact, LSEM sheet processed at $\lambda = 0.7$ with a strong B-fiber texture (Fig. 3b) and grain size of ~ 3 μm was found to exhibit up to 25% elongation to failure without compromise in the yield strength (170 MPa). *In situ* imaging of material flow under tensile loading further revealed the deformation to be highly uniform up to the point of fracture. This ability to sustain large uniform deformation is critical to sheet formability. On the other hand, rolled sheet with the basal texture failed at ~ 10% elongation, of which the uniform deformation was only 5%. Similarly, LSEM sheet tested under biaxial tensile loading, using a limiting dome height test, exhibited superior formability over the rolled sheet. Further work quantifying the texture/microstructure effects on Mg sheet formability is in progress, and will be part of a separate publication.

6. Summary

Large-strain extrusion machining (LSEM) was used to process Mg alloy AZ31B sheet in a single step of deformation with minimal external heating. High-speed image analysis showed that the deformation in LSEM can be approximated as simple shear along a plane, and the associated strain path can be varied by varying the shear plane orientation. Interestingly, it was found that the compressive field ahead of the shear deformation zone results in a deep twinned layer in the workpiece subsurface, reorienting the material entering the zone for basal and pyramidal $<c+a>$ slip. The intense shear deformation in LSEM resulted in close alignment of basal planes with the shear plane (i.e., B-fiber). This enabled varying the basal plane inclination from the sheet surface, in the range 32-53^{o}, by controlling the shear plane orientation. The B-fiber, associated with the basal slip, was found to be the major texture component over the range of deformation temperatures investigated. At elevated

temperatures, above ~ 300°C, an additional minor C_2-fiber was observed, indicating the activation of pyramidal $<c+a>$ slip with increasing temperature.

By controlling the *in situ* adiabatic heating in the deformation zone, microstructures ranging from heavily cold-worked to fully recrystallized type could be achieved. The corresponding grain sizes varied from UFG (100-500 nm) to conventional fine-grained (2-5 μm). Recovery-based continuous dynamic recrystallization was found to be the mechanism underlying the grain refinement.

The results show that LSEM offers opportunities for low-cost production of Mg sheet with improved combinations of formability and strength.

Acknowledgements
The authors would like to thank Dr. Yang Guo (M4 Sciences LLC) for help with the PIV analysis. The research was supported in part by US ARO grant W911NF-12-1-0012, and NSF grants CMMI 1100712 and 1234961.

References

[1] Hirsch J and Al-Samman T *Acta Mater.* 2013 **61** pp 818-843.
[2] Bohlen J, Nürnberg MR, Senn JW, Letzig D and Agnew SR *Acta Mater*. 2007 **55** pp 2101-2112.
[3] Beausir B, Suwas S, Tóth LS, Neale KW and Fundenberger JJ *Acta Mater.* 2008 **56** pp 200-214.
[4] Foley DC, Al-Maharbi M, Hartwig KT, Karaman I, Kecskes LJ and Mathaudhu SN *Scripta Mater*. 2011 **64** pp 193-196.
[5] Beausir B, Biswas S, Kim DL, Tóth LS and Suwas S *Acta Mater*. 2009 **57** pp 5061-5077.
[6] Yu Z, Choo H, Feng Z and Vogel SC *Scripta Mater*. 2010 **63** pp1112-1115.
[7] Efe M, Moscoso W, Trumble KP, Compton WD and Chandrasekar S *Acta Mater*. 2012 **60** pp 2031-2042.
[8] D Sagapuram, Efe M, Moscoso W, Chandrasekar S and Trumble KP *Acta Mater*. 2013 **61 pp** 6843-6856.
[9] Guo Y, Efe M, Moscoso W, Sagapuram D, Trumble KP and Chandrasekar S *Scripta Mater*. 2012 **66** pp 235-238.
[10] Adrian RJ *Annu. Rev. Fluid Mech.* 1991 **23** pp 261-304.
[11] Lutterotti L, Bortolotti M, Ischia G, Lonardelli I and Wenk HR *Zeitschrift für Kristallographie Suppl.* 2007 **26** pp 125-130.
[12] Guo Y, Saldana C, Compton WD and Chandrasekar S *Acta Mater*. 2011 **59** pp 4538-4547.
[13] Beausir B, Tóth LS and Neale KW *Acta Mater.* 2007 **55** pp 2695-2705.
[14] Reed-Hill RE and Robertson WD *Acta Metall.* 1957 **5** pp 728-737.
[15] Zheng B, Ertorer O, Li Y, Zhou Y, Mathaudhu SN, Tsao CY and Lavernia EJ *Mater. Sci. Eng.* A 2011 **528** pp 2180-2191.
[16] Chang C, Du XH and Huang JC *Scripta Mater*. 2008 **59** pp 356-359.
[17] Tan JC and Tan MJ *Mater. Sci. Eng.* A 2003 **339** pp 124-132.
[18] Gottstein G and Al-Samman T *Mater. Sci. Forum* 2005 **495** pp 623-632.
[19] Bozzolo N, Dewobroto N, Grosdidier T and Wagner F *Mater. Sci. Eng.* A 2005 **397** pp 346-355.
[20] Kim WJ and Sa YK *Scripta Mater.* 2006 **54** pp 1391-1395.